REPORT DOCUMENTATION PAGE

Form Approved
OMB No. 0704-0188

1. AGENCY USE ONLY *(Leave blank)*	2. REPORT DATE	3. REPORT TYPE AND DATES COVERED
	December 1992	Technical Paper

4. TITLE AND SUBTITLE
Aspects of Parking Orbit Selection in a Manned Mars Mission

5. FUNDING NUMBERS
WU 506-49-11-01

6. AUTHOR(S)
Prasun N. Desai, Robert D. Braun, and Richard W. Powell

7. PERFORMING ORGANIZATION NAME(S) AND ADDRESS(ES)
NASA Langley Research Center
Hampton, VA 23681-0001

8. PERFORMING ORGANIZATION REPORT NUMBER
L-17115

9. SPONSORING/MONITORING AGENCY NAME(S) AND ADDRESS(ES)
National Aeronautics and Space Administration
Washington, DC 20546-0001

10. SPONSORING/MONITORING AGENCY REPORT NUMBER
NASA TP-3256

11. SUPPLEMENTARY NOTES

12a. DISTRIBUTION/AVAILABILITY STATEMENT
Unclassified–Unlimited

Subject Category 13

12b. DISTRIBUTION CODE

13. ABSTRACT *(Maximum 200 words)*

For any round-trip Mars mission, the selection of a parking orbit at Mars must consider the precession caused by the oblateness of the planet. This precession will affect the departure condition for Earth return and, therefore, the initial mass required in low Earth orbit (LEO). In this investigation, which considers precession effects, minimum initial LEO masses were obtained for parking orbits characterized by having near-equatorial inclinations, high eccentricities, and three-dimensional departure burns (i.e., a burn with an in-plane and an out-of-plane velocity increment component). However, because near-equatorial inclination orbits have poor planetary coverage characteristics, they are not desirable from a science viewpoint. To enhance the potential for satisfying science requirements along with landing site accessibility, a penalty in the initial LEO mass is required. This study shows that there are a set of orbits characterized by low to moderate eccentricities ($e = 0.2$ to 0.5) and nonequatorial inclinations ($i = 70°$ to $140°$) that reduce this initial LEO mass penalty. Therefore, careful selection of a parking orbit at Mars can enhance the potential for satisfying science requirements with minimal mass penalties.

14. SUBJECT TERMS	15. NUMBER OF PAGES
Mars parking orbits; Manned mars mission; Nonspherical gravitational effects	27
	16. PRICE CODE: A03

17. SECURITY CLASSIFICATION OF REPORT	18. SECURITY CLASSIFICATION OF THIS PAGE	19. SECURITY CLASSIFICATION OF ABSTRACT	20. LIMITATION OF ABSTRACT
Unclassified	Unclassified		

NSN 7540-01-280-5500

Standard Form 298(Rev. 2-89)
Prescribed by ANSI Std. Z39-18
298-102

NASA-Langley, 1993

Acknowledgment

This technical report is a culmination of 1½ years of research in the Vehicle Analysis Branch of the Space Systems Division at NASA Langley Research Center (LaRC), during which time the authors have received technical guidance from numerous sources. We particularly wish to express appreciation to Gerald Walberg of North Carolina State University at Raleigh for providing valuable assistance and knowledge of manned Mars missions. Additionally, we would like to extend appreciation to James Buglia of Flight Mechanics and Control Inc., Hampton, VA, and Scott Striepe of LaRC for their technical comments and suggestions.

Use of Trademarks

Summary

For a manned Mars mission, the selection of a parking orbit is greatly influenced by the precession caused by the oblateness of the planet. This precession also affects the departure condition for Earth return and, therefore, the propellant and initial mass required in low Earth orbit (LEO). Additionally, the targeted parking orbit must also satisfy any science and landing site accessibility requirements that a mission might entail. Hence, the selection of a Mars parking orbit for a particular mission cannot be based purely on mission performance. Therefore, a trade-off between mission performance, science requirements, and landing site accessibility must be made.

In this investigation, an initial opposition-class mission with a 2017 Earth departure date, a total trip time of 1.6 years, and a 60-day Mars stay time was analyzed. Two parking orbit selection strategies were considered. First, a parametric study was performed, in which the inclination and eccentricity were varied to determine the velocity increments (ΔV values) for a range of Mars insertion and departure trajectories. Second, an *exact precession orbit* was sought. This orbit is defined as a parking orbit that would precess such that a tangential periapsis burn could be performed at both arrival and departure. This orbit selection strategy was initiated to minimize the arrival and departure ΔV values and simultaneously enhance the potential to satisfy any science requirements. Because the parking orbit obtained from the above two strategies affects the ascent and descent conditions for the Mars excursion module (MEM), the MEM mass was estimated for the various parking orbit inclinations and eccentricities. Thus, how the MEM affects the overall initial LEO mass can be better understood.

In the parametric study, a specific inclination and eccentricity of the parking orbit were targeted from the inbound interplanetary asymptote. After the 60-day stay time, a three-dimensional (3-D) departure burn (i.e., a burn with an in-plane and an out-of-plane ΔV component) was used at periapsis to achieve the proper outbound hyperbola for return to Earth. Additionally, the effect of departing from a location other than periapsis was also analyzed in this study. From these simulations, trends of initial LEO mass versus the inclination and eccentricity of the parking orbit were developed. For the exact precession study, the parking orbit inclination and eccentricity were optimally selected such that tangential periapsis burns could be performed at both arrival and departure in order to match the departure hyperbolic requirements. General perceptions suggest that an exact precession orbit should result in the lowest initial LEO mass for a given parking orbit eccentricity, because no change in direction of the arrival or departure velocity vector is required.

This investigation shows that the ΔV necessary to compensate for the precession of the parking orbit has a major effect on the initial LEO mass. As a result, the inclination and eccentricity of the parking orbit cannot be chosen arbitrarily, and a detailed analysis must be performed to obtain an optimum parking orbit. In this study, minimum initial LEO masses were obtained for Mars parking orbits characterized by having near-equatorial inclinations, high eccentricities, and a 3-D departure burn. Because they have poor planetary coverage characteristics, near-equatorial inclination orbits are not desirable from a science viewpoint. To enhance landing site accessibility and the potential for satisfying science requirements, a penalty in the initial LEO mass is required. This study shows that this initial LEO mass penalty can be minimized by using exact precession orbits characterized by low-to-moderate eccentricities ($e = 0.2$–0.5) and nonequatorial inclinations ($i = 70°$–$140°$). Additionally, this investigation also shows that the use of retrograde orbits, where $i > 90°$, can reduce the penalty in mission performance even with the increase in MEM mass associated with their use. Furthermore, the parametric results indicate that periapsis is not the optimum location for departure for most parking orbits. Therefore, the departure true anomaly along with the inclination and eccentricity of the parking orbit must also be considered in reducing the initial LEO mass.

Symbols

C_D	coefficient of drag
e	eccentricity
g	Earth's surface gravitational acceleration constant, 9.81 m/sec^2
h_p	periapsis altitude, km
I_{sp}	vacuum specific impulse, sec
i	inclination, deg
$\hat{i}, \hat{j}, \hat{k}$	unit vector along the inertial X, Y, and Z axes, respectively
J_n	zonal coefficients
L	geocentric latitude, deg
M	spacecraft mass, kg
M_i/M_f	ratio of initial LEO to final LEO spacecraft mass

m_f	spacecraft mass just after propulsive maneuver, kg
m_i	spacecraft mass prior to propulsive maneuver, kg
P_n	Legendre polynomials
r	position of spacecraft, m
$\mathbf{r}$	position vector of spacecraft, m
r_{eq}	equatorial radius of Mars, m
T/W	ratio of engine thrust to weight
t	time, sec
U	gravitational potential
V_∞	hyperbolic excess velocity, km/sec
x, y, z	inertial planetocentric position in Cartesian coordinates, m
α	right ascension, deg
β	out-of-orbital-plane angle defining the departure burn direction, deg
ΔV	velocity increment, km/sec
ΔV_{dep}	velocity increment at departure, km/sec
ΔV_{ins}	velocity increment at insertion, km/sec
δ	declination, deg
δ_{arr}	arrival declination, deg
δ_{dep}	departure declination, deg
δ_{max}	maximum declination between δ_{arr} and δ_{dep}, deg
γ	in-plane angle defining the departure burn direction, deg
μ	gravitational parameter of Mars, m^3/sec^2
Ω	longitude of ascending node, deg
ω	argument of periapsis, deg
θ	true anomaly, deg

Abbreviations:

COSPAR	Committee on Space Research
LEO	low Earth orbit
LH_2	liquid hydrogen
LOX	liquid oxygen
MEM	Mars excursion module
POST	Program to Optimize Simulated Trajectories
SOI	sphere of influence
Sol	orbit with a period of one solar day
SWISTO	Swingby-Stopover Optimization Program
3-D	three-dimensional

Introduction

Background and Objectives

The Sally Ride report "Leadership and America's Future in Space" (ref. 1) and President Bush's speech at the 20th anniversary of the Apollo Moon Landing have sparked a renewed interest in a manned mission to Mars in the early 21st century. Recent studies have shown that numerous opportunities exist in the 2010–2025 time frame for a chemically propelled, high-thrust vehicle to perform a 1–2-year round-trip mission that includes a 60-day stay time (refs. 2–5). Although a significant amount of research has been directed toward determining optimum interplanetary trajectories for an Earth–Mars manned mission, less effort has been devoted to determining an appropriate Mars parking orbit. Therefore, the primary focus of this study is to determine the effects of Mars parking orbit selection on the overall mission profile. In particular, parking orbit selection dictates the propulsive requirements necessary for injection into and departure from Mars orbit. A poor selection may result in an increase in the initial low Earth orbit (LEO) spacecraft mass of 30–100 percent over an ideal case (refs. 6 and 7).

Previous studies have focused on determining the effects of Mars parking orbits on the overall mission profile (refs. 6 and 7). However, most of the analyses that were performed were based only on orbital energy (i.e., the eccentricity of the parking orbit for a given periapsis altitude). Detailed approach and departure geometries of the parking orbit were not taken into account. Furthermore, in most studies, a spherical gravitational potential for Mars was assumed; precession of the parking orbit (caused by the oblateness of Mars) was not considered in the analyses. Without precession, the arrival orbital geometry remains fixed throughout the length of the stay time. Therefore, the actual departure geometry was not employed in these studies (refs. 2–7). Also in these analyses, the departure burn for return to Earth was assumed to be tangential; however, in actuality, geometrical constraints may require this burn to be 3-D

(i.e., a burn with an in-plane and an out-of-plane velocity increment (ΔV) component). As a result, these preliminary studies produced optimistic estimates of the arrival and departure burns and, hence, the initial LEO mass. Additionally, these studies did not significantly assess the impacts of scientific requirements (i.e., orbital observations or landing site accessibility) on the Mars mission profile. Thus, in these studies, the choice of the parking orbit was based purely on mission performance (initial LEO mass). To obtain a more realistic initial LEO mass, a detailed analysis of the parking orbit is required.

The primary objective of this investigation was to identify trends and aspects of Mars parking orbits for an initial manned mission. In particular, parking orbit selection required a thorough analysis of the following parameters: (1) scientific requirements, (2) landing site accessibility, (3) length-of-stay time, (4) inclination, (5) periapsis altitude, and (6) eccentricity. Furthermore, the effects of orbital precession resulting from the oblateness of Mars were also considered. A gravitational model that realistically accounts for this oblateness was used to better assess the actual resulting geometries caused by the precession of the parking orbit. Hence, the parking orbit no longer remains fixed throughout the length-of-stay time but precesses from arrival to departure. Also in this strategy, the departure burn was allowed to vary three-dimensionally as required to satisfy the constraints imposed by the outbound hyperbolic trajectory.

A second objective of this study was to identify parking orbits that would precess so that tangential periapsis burns could be performed at both arrival and departure, as was assumed in the previous studies (refs. 2–7). Because the present study takes into account the precession effects caused by an oblate Mars on the parking orbit, the resulting geometries at arrival and departure were realistically simulated to obtain these minimum burn parking orbits. This orbit selection strategy was initiated to minimize the initial LEO mass and simultaneously enhance the potential to satisfy any science requirements.

Because the parking orbit obtained from the above two strategies affects the ascent and descent conditions for the Mars excursion module (MEM), the MEM mass must be analyzed for the various parking orbit inclinations and eccentricities. In so doing, the effects of the MEM mass on the overall mission profile (hence, the initial LEO mass) can be better understood.

Vehicle Characteristics and Mission Scenario

The baseline vehicle and interplanetary mission profile are based on the requirements of an initial manned exploration scenario (refs. 2–4). The interplanetary transfer vehicle used in this analysis is similar to that developed by Tucker et al. (fig. 1 and ref. 8), and its mass breakdown is given in table 1. Note that a range of Mars excursion module (MEM) masses is given, which was calculated for the various parking orbit characteristics considered in this analysis. In this study, liquid oxygen/liquid hydrogen (LOX/LH_2) rocket engines with a vacuum specific impulse (I_{sp}) of 480 sec were used for the transfer vehicle, and the corresponding tankage mass for the transfer vehicle and the MEM was assumed to be 10 percent of the required propellant mass. The two habitation modules of the spacecraft, which have been adapted from space station hardware, are attached to either end of a rotating truss structure to provide an artificial gravity environment. Also included aboard the interplanetary transfer vehicle is the MEM. The MEM, whose characteristics are given in table 2, comprises all vehicle components required for descent to, exploration of, and ascent from the Martian surface.

The mission scenario, which was adopted for the present study, is described as follows. The interplanetary transfer vehicle departs from a circular low Earth orbit (h_p = 500 km). Upon arrival at Mars, the vehicle performs a tangential burn (ΔV_1) to the inertial planetocentric velocity vector at periapsis of the approach hyperbola for insertion into a parking orbit (fig. 2(a)). Following insertion, the MEM separates from the interplanetary transfer vehicle and then using ΔV_2, circularizes at the periapsis altitude (fig. 2(b)). Once circularization is completed, the MEM descends to the Martian surface via ΔV_3. After performing the necessary excursion operations, the MEM ascends to a phasing orbit where an apoapsis burn (ΔV_4) is performed so that rendezvous with the interplanetary transfer vehicle can occur in the parking orbit (fig. 2(c)). At the end of the 60-day stay time, the MEM is discarded and a departure burn, ΔV_5 (tangential or 3-D), is performed at some true anomaly (θ) for Earth return (fig. 2(d)). Upon Earth arrival, the habitation modules and support structure are discarded before the propulsive maneuver for Earth-orbit insertion, and only the manned capsule (ref. 9) is inserted into an orbit with a period of one Earth day (1 Sol) and at h_p = 500 km. Note that the appropriate propellant tankage is discarded after each burn.

Analysis

Interplanetary Trajectory and Parking Orbit Characteristics

Because the analysis of interplanetary trajectory and parking orbit characteristics is performed through a series of mass-ratio calculations, the results presented apply to any vehicle design provided that three conditions remain nearly constant: (1) the propulsion systems must be similar in terms of I_{sp} and tank-mass fraction, (2) the ratio of mass left behind at Mars to Earth return payload must be comparable, and (3) the use of impulsive velocity additions is valid. The mass ratio (M_i/M_f) represents the mass in kilograms that must be placed initially into LEO for every kilogram of mass returned to LEO at the end of the mission. For example, the vehicle described in the analysis has a mass of 6.8×10^3 kg at Earth return. Thus, a M_i/M_f of 150 would require an initial LEO mass of 1.02×10^6 kg.

The parking orbit analysis was performed for the interplanetary mission profile that is described in the Introduction and has the following dates (fig. 3):

Chart A

Earth departure	April 4, 2017
Venus swingby	September 9, 2017
Mars arrival	March 23, 2018
Mars departure	May 22, 2018
Earth arrival	November 13, 2018

This profile is for a typical opposition-class mission taken from the set of opportunities presented in reference 2. It includes a Venus swingby on the outbound Earth–Mars trajectory leg and has a total trip time of 1.6 years. For this mission profile, the ΔV values for Earth departure and arrival are 4.17 km/sec and 1.13 km/sec, respectively. The arrival and departure hyperbolic excess velocity vectors at Mars can be described (with respect to Mars) in terms of right ascension (α), declination (δ), and hyperbolic excess velocity (V_∞) as follows:

Chart B

Arrival	Departure
$\alpha = 253.99^\circ$	$\alpha = 212.57^\circ$
$\delta = -21.4^\circ$	$\delta = -12.5^\circ$
$V_\infty = 5.441$ km/sec	$V_\infty = 3.873$ km/sec

These interplanetary conditions were generated with the Swingby-Stopover Optimization Program (SWISTO) (ref. 10), which uses a 3-D patched conic approach. As a result of the patch-conic two-body approximation, the position vector at the sphere of influence (SOI) is not uniquely defined. Therefore, numerous parking orbit inclinations may be achieved. However, as Tolson (ref. 11) demonstrated for any hyperbolic approach, if only a tangential burn is performed, the arrival declination (δ_{arr}) of the velocity vector limits the achievable parking orbit inclination. The advantage of using a tangential burn over a 3-D burn is that no change in direction of the velocity vector is required, thus reducing the size of the burn and, hence, the initial LEO mass. Therefore, one of the objectives of this study was to obtain parking orbits that used tangential burns. As a result, the achievable range of orbital inclinations (i) at arrival is

$$|\delta_{\text{arr}}| \le i \le 180^\circ - |\delta_{\text{arr}}|$$

However, because of the round-trip mission profile, the orbital geometry at Mars departure also needs to be considered in the selection of the parking orbit inclination. To achieve the departure hyperbolic asymptote with a tangential burn, the parking orbit inclination at the end of the stay time has to be greater than or equal to the departure declination (δ_{dep}) of the hyperbolic asymptote or less than or equal to 180° minus the declination. That is, the possible range of orbital inclinations at departure is

$$|\delta_{\text{dep}}| \le i \le 180^\circ - |\delta_{\text{dep}}|$$

This criterion adds another restriction on the possible range of parking orbit inclinations. Therefore, accounting for both arrival and departure geometries and the use of tangential burns, the achievable range of parking orbit inclinations is determined by the maximum declination (δ_{max}) between the arrival and departure velocity vectors. Hence, the achievable range of orbital inclinations for a round-trip mission using tangential burns upon arrival and departure is

$$|\delta_{\text{max}}| \le i \le 180^\circ - |\delta_{\text{max}}|$$

For this mission profile, any inclinations between 21.4° and 158.6° were possible, based on $\delta_{\text{arr}} = 21.4^\circ$. If inclinations beyond this range are desired, either a 3-D burn upon arrival or an additional propulsive maneuver after orbit insertion is required. In addition, an upper limit on the period of the parking orbit of one Martian day (1 Sol) was also imposed because of concerns that an orbit with a longer period would result in the MEM approaching escape velocity during the ascent and rendezvous phases. This orbital period limitation constrains the eccentricities allowed

in the parking orbit. As a result, the various inclinations (i) and eccentricities (e) considered in the parametric portion of this analysis were as follows:

$i = 21.5°, 40°, 60°, 75°, 90°, 105°, 125°, 145°,$ and $158.5°$

$e = 0.05, .25, .50, .75, .809$ ($h_p = 500$ km, 1 Sol), and $.821$ ($h_p = 250$ km, 1 Sol)

This analysis was performed for periapsis altitudes of 250 km and 500 km. These altitudes were selected for consistency with sizing and mass estimates of the MEM subsystems (ref. 7).

Trajectory Simulation: Parking Orbit Targeting

A parametric study was first performed in this analysis, where the inclination and eccentricity of the parking orbit were varied to determine the ΔV values for Mars insertion and departure trajectories. For this strategy, trends of initial LEO mass versus inclination and eccentricity were developed. Secondly, an *exact precession orbit* was sought. This orbit is defined as a parking orbit that would precess such that a tangential periapsis burn could be performed at both arrival and departure. General perceptions suggest that an exact precession orbit should result in the lowest initial LEO mass for a given parking orbit eccentricity, because no change in direction of the arrival or the departure velocity vector would be required.

In the parametric study, specific inclination and eccentricity of the parking orbit were targeted from the arrival interplanetary asymptote at the sphere of influence (SOI). After the 60-day stay time, a 3-D departure burn was used at periapsis to achieve the proper departure hyperbola for Earth return. By selecting the parking orbit inclination and eccentricity, the initial position on the edge of the SOI for the arrival asymptote was fixed. Thus, this problem was defined by three constraints (the right ascension (α), declination (δ), and the magnitude (V_∞) of the departure hyperbolic excess velocity vector at the SOI) and three control variables (the in-plane (γ) and out-of-orbital-plane (β) angles defining the departure burn direction and the magnitude of the departure burn (ΔV). The effect of departing from a location other than periapsis was also analyzed in this study. This strategy added an additional control, the true anomaly at departure (θ), to the definition of the problem stated above.

For the exact precession study, the initial position on the SOI (therefore, inclination of the parking orbit), the energy of the parking orbit (hence, its eccentricity, knowing the periapsis altitude), and the magnitude of the tangential periapsis departure burn were optimally selected to match the requirements of the departure hyperbola. Because the parking orbit inclination and eccentricity were not specified, the initial position on the edge of the SOI and the energy of the parking orbit were variable. This condition added three controls and one constraint to the targeting process. The three controls were the energy of the parking orbit and two of the three position variables x, y, or z. The third variable can be determined from the other two and the magnitude of the SOI radius from the planet because the position vector must be at the SOI. The one constraint was the periapsis altitude. Because the departure burn direction was fixed (tangential), two controls (γ and β) were eliminated from the targeting process and only the magnitude of the departure burn remained a variable. Therefore, this exact precession problem was defined by four constraints (α, δ, and V_∞ for the departure hyperbolic asymptote and the periapsis altitude of the parking orbit) and four control variables (x, y, energy of parking orbit, and departure ΔV).

In this manner, Mars arrival and departure ΔV values were obtained. With all the ΔV values now defined (i.e., for Earth departure, Mars arrival, Mars departure, and Earth arrival) and the dry mass of the vehicle known (table 1), the rocket equation may be used to determine the propellant requirements of the vehicle and, thus, the initial LEO mass of the vehicle. The rocket equation can be expressed as

$$\Delta V = I_{sp}\ g\ \ln\left(m_i/m_f\right)$$

where I_{sp} is the vacuum specific impulsive, g is the Earth's surface gravitational acceleration, and m_i and m_f are the spacecraft masses prior to and just after the propulsive maneuver (ΔV), respectively. Note that losses due to all external forces (e.g., gravity, drag, thrust misalignment, etc.) in the rocket equation were neglected in the determination of the initial mass of the vehicle in LEO.

Mars Excursion Module

To realistically model the effects of the various Mars parking orbit characteristics (i.e., inclinations and eccentricities), ascent and descent trajectory simulations for the MEM were calculated for numerous inclinations, eccentricities, and periapsis altitudes. Thus, the variation in the MEM mass shown in table 1 is a result of these various parking orbit characteristics. The propellant and tankage masses required for each of these cases were then included in

the calculation of the entire interplanetary transfer vehicle mass in LEO.

Descent trajectory. Descent to the Martian surface was simulated as follows (fig. 2(b)): After a parking orbit was established, the descent to the surface was accomplished by separating the MEM from the interplanetary transfer vehicle and performing a circularization burn (ΔV_2) at periapsis. Circularization of the MEM orbit is desirable before deorbiting because the ΔV to deorbit is the same for any point within this orbit. This strategy allows the MEM to descend to the northern as well as southern latitudes, and provides a day or night landing capability without a significant cross-range requirement, as long as the landing site latitude is less than the inclination of the parking orbit. By circularizing the orbit, the descent is decoupled from the orbital insertion maneuver. This procedure allows greater access to the Martian surface because the descent geometry is no longer fixed as is the case for a direct descent from the parking orbit. For direct descent from the parking orbit, the periapsis of the parking orbit must be over the landing site latitude. This requirement places an additional demand on the orbital geometry between the arrival hyperbolic asymptote and the parking orbit and could severely restrict the number of possible Mars parking orbits. Therefore, circularizing the MEM orbit increases mission flexibility. Once circularization is complete, a deorbit burn (ΔV_3) is performed to initiate the entry and landing sequence. Deorbit ΔV values and the propellant usage were calculated with the assumption of a Hohmann transfer from the current circular orbit to a transfer orbit with a zero vacuum periapsis altitude (i.e., no atmosphere was assumed for Mars). A 10-percent margin was assumed in all descent ΔV values to account for the fuel required for retro firing at touchdown and any other incidental burns during descent.

Ascent trajectory. To simplify the ascent analysis, an equatorial landing site was arbitrarily assumed so that rendezvous with the interplanetary transfer vehicle left in the parking orbit (fig. 2(c)) can be accomplished over the entire range of inclinations considered in this study. This assumption imposes a maximum penalty, in terms of ΔV, for a retrograde (due west) launch, whereas a minimum estimate of ΔV is obtained for a direct (due east) launch as a result of the planet's rotation. For nonequatorial landing sites, the ascent ΔV would fall between the estimates mentioned above. A pitch rate steering guidance law was used to simulate the ascent trajectory for a single-stage vehicle which maximized the MEM mass inserted into a phasing orbit. Once in orbit at this intermediate altitude, the MEM performed a Hohmann transfer burn (ΔV_4) at apoapsis to achieve the parking orbit of the transfer vehicle for rendezvous. The Martian atmosphere was simulated with the Committee on Space Research (COSPAR) northern hemisphere summer mean density model (ref. 2) whereas coefficient of drag (C_D) versus Mach number of the Apollo capsule was used to approximate the MEM aerodynamics (ref. 12). A 10-percent margin was also assumed in all ascent ΔV values to account for any burns required during rendezvous.

Using the MEM characteristics shown in table 2, a parametric study of inclination, eccentricity, and periapsis altitude was performed, from which ascent and descent ΔV values were determined. The rocket equation was then used to obtain the mass of the MEM for these various parking orbit characteristics.

Gravitational Model

The acceleration of a spacecraft acted upon by a central attracting body is

$$\frac{d^2\mathbf{r}}{dt^2} = \nabla U = \frac{\partial U}{\partial x}\hat{i} + \frac{\partial U}{\partial y}\hat{j} + \frac{\partial U}{\partial z}\hat{k}$$

where $\mathbf{r}$ is the position of the spacecraft, t is time, and U is the gravitational potential.

The gravitational potential for a spherically symmetric mass body is μ/r. However, Mars is not spherically symmetric but is bulged at the equator and flattened at the poles, similar to Earth. To account for this nonuniform mass distribution, the following potential was used:

$$U = \frac{\mu}{r}\left[1 - \sum_{n=2}^{\infty}\left(\frac{r_{\mathrm{eq}}}{r}\right)^n J_n P_n(\sin L)\right]$$

where μ and r_{eq} are the gravitational parameter and equatorial radius of Mars, respectively, J_n are the zonal coefficients, P_n are Legendre polynomials, and L is the geocentric latitude (ref. 13).

The above potential considers only the effects of the zonal harmonics, which are the dominant harmonics for Mars. These harmonics take into account the mass distribution that is rotationally symmetric about the north-south axis (i.e., the harmonics are

latitude dependent only). The numerical values used for the zonal coefficients in this analysis for Mars are:

$$J_2 = 1.9595 \times 10^{-3}$$

$$J_3 = 3.5837 \times 10^{-5}$$

$$J_4 = -1.1772 \times 10^{-5}$$

$$J_5 = 9.0793 \times 10^{-6}$$

$$J_6 = -3.1549 \times 10^{-7}$$

Normalized zonal coefficients were obtained from references 14–16, averaged, and then unnormalized by Kaula's rule of thumb (ref. 17) to produce the above values. In these references, the zonal coefficients for Mars were determined by tracking the Mariner 9 space probe and the Viking 1 and 2 spacecraft orbiting the planet. Figure 4 shows schematically the geometrical shape associated with each of these zonal coefficients J_n. The largest term for Earth and Mars is J_2, which indicates the flattening of the planet (i.e., it accounts for the equatorial bulge). The J_3 term corresponds to a tendency toward a triangular shape, J_4 toward a square shape, and so forth. Of note is that all the geometrical shapes depicted are positive zonal coefficients. By superimposing these harmonics, it is possible to approximate any gravitational field that is symmetric about the polar axis.

Computational Tools

Program to Optimize Simulated Trajectories (POST). The orbital and ascent analyses in this study were performed with the Program to Optimize Simulated Trajectories (POST) (ref. 18). POST was initially developed by the Martin Marietta Corporation as a Space Shuttle trajectory optimization program. Since that time, POST has been used to solve a wide variety of atmospheric ascent, reentry, and orbital transfer problems near an arbitrary, rotating, oblate planet, where the equations of motion within POST are integrated numerically. By perturbing the independent variables (controls) with respect to each dependent variable (constraint) from an initial estimate of the controls, partial derivatives are determined and a projected gradient method is used to improve the controls in order to solve (target) the particular problem. Targeting occurs when the constraints are satisfied within the user-specified tolerances.

Semianalytic methods. Since this work was completed, semianalytic approaches of solving these types of problems have been developed which can reduce the computation time of the analyses (refs. 19–21). These approaches in references 19–21 consider the actual geometry between the arrival and departure hyperbolic asymptotes and the parking orbit, along with the precession effects caused by the oblateness of Mars, in calculating the arrival and departure ΔV values. References 19 and 20 describe the calculation of Mars parking orbits that use either (1) a tangential periapsis arrival burn and an in-plane departure burn, (2) an in-plane arrival burn and an in-plane departure burn, or (3) a tangential periapsis arrival burn and a 3-D departure burn, as in the case of the parametric strategy of the present study. Reference 21 describes the calculation of Mars parking orbits that uses tangential periapsis burns at both arrival and departure, as in the case of the exact precession strategy of the present study.

Results and Discussion

Effects of Oblateness

Previous studies have assumed Mars to be a spherical planet in order to obtain an initial estimate of a vehicle's initial mass in LEO (refs. 2–6, 8, and 22). Under this assumption, a parking orbit will not precess and, thus, will remain in the same plane at departure as it was in upon arrival (fig. 5). Because Mars is oblate, the parking orbit will precess, which results in a different departure plane (fig. 6). This change in the departure condition may drastically affect the Mars departure ΔV for Earth return and, therefore, the initial LEO mass of the vehicle. Table 3 shows a comparison between a previous study that neglected precession (ref. 2) and the present study, which includes precession. As seen, a large increase in the LEO mass (about 50 percent) is required for the same parking orbit, when the actual departure geometry is considered. Thus, the incorrect assumption of using a spherical planet in these previous studies could produce a misleading estimate of the initial LEO mass. Hence, to obtain a more realistic determination of the mass of a vehicle in LEO, precession effects need to be considered in any orbital analyses.

Because the longitude of ascending node and the argument of periapsis determine the orientation of the parking orbit about the planet, their motion affects the departure conditions for Earth return and, hence, the initial LEO mass. The two most significant effects of oblateness on an orbit are the movement of the longitude of ascending node and the argument of periapsis. The parameters that effect these motions are the eccentricity, inclination, and

periapsis altitude of the parking orbit, along with the length of the stay time. Figures 7 and 8 show the change in the longitude of ascending node (Ω) and the argument of periapsis (ω), respectively, versus eccentricity for various inclinations for a 30-day Mars stay time. As seen from these figures, the lower the eccentricity of the orbit and the more equatorial the inclination (i.e., for a very low or high inclination), the higher the precession of Ω and ω. The effect of periapsis altitude on ω is shown in figure 9, where again the lower the eccentricity of the orbit and the lower the periapsis altitude, the higher the precession. To first order, the longitude of ascending node and the argument of periapsis change linearly with time; hence, the longer the stay time, the greater the change. Therefore, knowledge of how a parking orbit precesses is essential in minimizing the initial LEO mass of the vehicle.

Ascent and Descent of the MEM

Ascent and descent ΔV calculations for the MEM are shown in figures 10–12 for periapsis altitudes of 500 km and 250 km. Figure 10 shows a near linear variation in descent ΔV with eccentricity; that is, the higher the eccentricity of the parking orbit, the greater the descent ΔV required. Figures 11 and 12 show the influence of inclination for the various eccentricities on the required ascent ΔV. As seen, the ascent ΔV increases with inclination, as expected. This increase in ΔV is a consequence of the rotational velocity of the planet. For low inclinations, smaller ΔV values are required because the ascent is in the same direction as the planet's rotation. However, as the inclination increases, a smaller component of the planet's rotational velocity aids in the ascent. As the inclination exceeds 90° (retrograde orbit), the planet's rotational velocity is in the opposite direction compared with the ascent and, hence, becomes a detriment. As a result, larger and larger ΔV values are required to overcome the planet's rotational velocity for launch. Additionally, figures 11 and 12 show that as the eccentricity increases, larger ΔV values are needed on account of the increased energy requirements of the parking orbits.

With these ΔV values and the MEM characteristics in table 2, MEM masses were calculated and are shown in figures 13 and 14. A similar trend in the MEM mass versus inclination and eccentricity of the parking orbit is observed, as compared with the ascent ΔV values of figures 11 and 12. From figures 11 and 12, a maximum penalty of about 0.6 km/sec is imposed on a due west launch when compared with a due east launch. This penalty translates into a maximum increase of about 13 500 kg in the MEM mass (for the 1-Sol orbit) as shown in figures 13 and 14. As seen from these figures, inclination does have some impact on the mass of the MEM. However, as shown later, this impact is insignificant compared with the overall mass of the entire vehicle initially in low Earth orbit. In fact, the Mars departure ΔV is the main driver in determining the parking orbit. Therefore, the consideration of a parking orbit need not be limited to only direct orbits, but should be expanded to include retrograde orbits. Additionally, the figures also show that periapsis altitude does not significantly affect either the ascent and descent ΔV values or the MEM mass.

Parametric Study

Figures 15 through 20 show the vehicle mass ratio in LEO (M_i/M_f) versus inclination for various eccentricities and departure conditions. One clarification needs to be made about figures 15–20. The curves displayed are the best possible match to the data. For the higher eccentricities, continuous curves are shown. However, for the low eccentric orbits, only computed points are displayed because exact curve fits were not possible on account of the large variation in the data. If calculations were made with a smaller increment in inclination (for the lower eccentricities), the computed points would fall closer together and result in a smooth curve fit.

Figures 15 and 16 show a large variation in the mass ratio in LEO for a periapsis departure from the parking orbits considered. As seen in these two figures, certain combinations of the orbital parameters (especially those with low eccentricity) induce a drastic mass-ratio penalty. Ranges in M_i/M_f from about 150 to 1900 are seen for these two periapsis altitudes. This result suggests that periapsis (true anomaly of 0°) is not typically the optimum location for a departure burn. Therefore, the parametric analysis was repeated to determine the effect of true anomaly on minimizing the departure ΔV (hence, the mass ratio).

The results from an optimization of the departure location, or true anomaly, are shown in figures 17 and 18. As seen from these figures, M_i/M_f has been drastically reduced from an initial range of 150–1900 to a new range of 140–450, and, indeed, periapsis is not the best location for a departure burn for most of the orbits. However, in the search for the best departure location, an optimization problem within POST was encountered. Many local minima were found which complicated the search for the departure true anomaly that resulted in a minimum departure ΔV. Therefore, a global minimum was not always found. Figure 19 shows this effect for the

$e = 0.75$ curve from figure 17. Using different initial conditions, the analysis was repeated for the first two points ($i = 21.5°$ and $40°$). As seen, much lower mass ratios were produced and, hence, a more favorable departure location, or true anomaly. Therefore, to obtain exact and precise plots of the LEO mass ratio, a parametric study in true anomaly must also be performed along with inclination and eccentricity to determine the minimum departure ΔV. Because many local minima exist, a better global optimizer is necessary to determine the optimum true anomaly that yields the minimum departure ΔV.

As a result of this behavior, a parametric study in true anomaly was performed for three inclinations ($i = 21.5°$, $90°$, and $158.5°$) for the 1-Sol parking orbit with a periapsis altitude of 500 km ($e = 0.809$). Figure 20 shows the results for periapsis departure (from fig. 15) and those for an optimized departure location. As seen, a penalty is imposed when a periapsis departure is required in this mission profile. The size of this penalty depends upon the inclination of the orbit. In this case, a large penalty in the LEO mass ratio is imposed for inclinations less than $90°$.

Figure 20 also shows that for the optimized departure curve, lower values of the mass ratio in LEO are obtained for both posigrade and retrograde orbits with near-equatorial inclinations (i.e., for very low or high inclinations). As a result, these orbits are favorable from the point of view of mission performance (i.e., lower mass ratio). However, because of their limited planetary coverage, equatorial orbits display poor characteristics for scientific observations and landing site accessibility. Therefore, if a non-equatorial orbit is required to improve the potential for satisfying scientific and landing site requirements, a penalty in mission performance (i.e., higher mass ratio) is induced. For example, to achieve a polar orbit, an increase in M_i/M_f of approximately 50 percent is required, as seen in figure 20.

In summary, a few general statements concerning parking orbit selection can be made from these parametric results: (1) Periapsis altitude does not have a major impact on the LEO mass ratio, as seen in figures 17 and 18. Most values of M_i/M_f are in the range from 150 to 300 for both altitudes. Because a variation in the mass ratio is present, the choice of a parking orbit cannot be made arbitrarily, and a thorough analysis is required to minimize the initial LEO mass. (2) No one particular eccentricity is favorable for the entire range of inclinations. In fact, a low eccentricity ($e = 0.50$) is favored over a high eccentricity ($e = 0.75$ or 1-Sol orbit) for intermediate inclinations ($i \approx 45°$–$85°$) for both periapsis altitudes. (3) Periapsis is not necessarily the optimum location for a departure burn for a majority of the orbits as shown in figure 20. (4) Also from figure 20, a retrograde parking orbit ($i = 158.5°$) can result in a lower mass ratio than a direct orbit ($i = 21.5°$). Therefore, the increase in the MEM mass associated with retrograde orbits is not of enough significance to disallow their use.

Exact Precession Study

One way of minimizing the penalty in mission performance, while still achieving scientific requirements, is to search for an *exact precession parking orbit*; that is, a parking orbit that precesses such that a tangential periapsis burn can be performed at both arrival and departure. General perceptions suggest that this tangential, periapsis-to-periapsis transfer (for a given parking orbit eccentricity) would result in the lowest initial LEO mass, because no change in the direction of the arrival or departure velocity vector is required.

From this study, only a finite number of exact precession orbits were found to exist. The problem in using exact precession orbits arises from the requirement that an alignment of the argument of periapsis (ω), the longitude of ascending node (Ω), and the true anomaly (θ) is necessary before a tangential departure burn can be performed at periapsis. Because these elements precess at different rates, there are only a few combinations of these parameters that result in a tangential periapsis departure burn for a given stay time and periapsis altitude. For example, consider a parking orbit ($h_p = 250$ km) with a stay time of 60 days and an inclination of $90°$ (a polar orbit) such that the arrival (initial) and departure (final) Ω, ω, and θ are

Chart C

Initial	Final
$\Omega = 253.9°$	$\Omega = 32.6°$
$\omega = 265.2°$	$\omega = 76.4°$
$\theta = 0°$	$\theta = 0°$

in order to perform a tangential periapsis burn upon arrival and departure. An eccentricity for the parking orbit may exist that will regress the argument of periapsis such that, at departure, $\omega = 76.4°$. However, because the longitude of ascending node does not precess for a parking orbit with an $i = 90°$ (for the gravity model used in this analysis), as shown in figure 7, there is no eccentricity that will rotate the longitude of ascending node from $\Omega = 253.9°$ at arrival to $\Omega = 32.6°$ at departure. Therefore, an exact precession parking orbit, which precesses both

the longitude of ascending node and the argument of periapsis such that a tangential periapsis burn can be performed upon arrival and departure, is not possible for this inclination.

For other inclinations, an eccentricity that changes the longitude of ascending node to its departure value may be obtained; however, this eccentricity most likely will not change the argument of periapsis to its departure value because it precesses at a different rate than the longitude of ascending node. As an example, consider a parking orbit ($h_p = 500$ km) with a stay time of 60 days and $i = 30°$, where the initial and final conditions for a tangential periapsis burn are

Chart D

Initial	Final
$\Omega = 296.7°$	$\Omega = 10.1°$
$\omega = 238.9°$	$\omega = 90.5°$
$\theta = 0°$	$\theta = 0°$

For this parking orbit, $e = 0.135$ causes Ω to regress to its final value of 10.1°. However, the value of ω (for this inclination) at the end of the stay time is 330.6°, and, once again, an exact precession parking orbit is not possible because the two elements (Ω and ω) precess at different rates. As a result of this difficulty, only a limited number of inclinations and eccentricities will produce an exact precession orbit. Therefore, the determination of the inclination and eccentricity that yields an exact precession orbit is complicated because numerous combinations of inclinations and eccentricities must be examined. The true anomaly criterion ($\theta = 0°$ at arrival and departure) is necessary for the determination of an exact precession orbit. However, this criterion is not difficult to satisfy because θ is an independent variable and, therefore, does not explicitly depend on the inclination or eccentricity of the parking orbit.

In this study, nine exact precession orbits were found, five for a periapsis altitude of 500 km and four for a periapsis altitude of 250 km (for this interplanetary mission profile). Tables 4 and 5 list the various characteristics of these orbits and other orbits of interest (from the parametric results) for the two periapsis altitudes. Note that the orbits are numbered for reference. As seen in tables 4 and 5, exact precession orbits occur only at low to moderate eccentricities, ranging from near circular ($e = 0$) to about 0.44, for this mission profile. This outcome is a consequence of the requirement for a proper alignment of Ω, ω, and θ, where the need for sufficient precession of these parameters (required for a proper alignment) drives the eccentricity of exact precession orbits toward zero. As a result, exact precession orbits tend to be low-energy orbits.

Comparison of the orbits given in tables 4 and 5 shows that exact precession orbits can result in low mass ratios. However, for the mission profile used in this analysis, an exact precession orbit was not found to yield the absolute minimum mass ratio, even with the use of tangential periapsis burns, which is contrary to general perception. This result is due to the lower energy state of exact precession orbits, thus requiring larger ΔV values than for some of the 1-Sol (higher energy) orbits. Therefore, from these results, an exact precession orbit should not necessarily be selected if minimizing the mass ratio in LEO is the main objective of the mission. For this interplanetary mission profile, 1-Sol orbits with an inclination of 158.5° and 3-D departure burns yield minimum mass ratios of 141.5 and 138.8 for periapsis altitudes of 500 km and 250 km, respectively. However, because these orbits are near-equatorial, they may be poor selections from a scientific standpoint and limit the choice of potential landing sites. Therefore, a penalty in mission performance is required to obtain a more favorable inclination for these science requirements. In comparison with the $i = 158.5°$, 1-Sol orbit ($e = 0.809$ and 0.821), figures 21 and 22 show the percent increase in the LEO mass ratio required for achieving the various parking orbits listed in tables 4 and 5 for the two periapsis altitudes. For example, to achieve a more favorable inclination from a scientific standpoint, increases in M_i/M_f of 46.1 percent (orbit no. 9 in fig. 21) and 49.6 percent (orbit no. 8 in fig. 22) are imposed for achieving a polar orbit for periapsis altitudes of 500 km and 250 km, respectively.

The advantages of using exact precession orbits are that lower eccentricities and more favorable inclinations are possible without a drastic penalty in mission performance. Penalties of only 2.7 percent and 0.07 percent in M_i/M_f are required for the exact precession orbits with $i = 70.7°$, $e = 0.381$, $h_p = 500$ km (orbit no. 1 in fig. 21) and $i = 71.1°$, $e = 0.436$, $h_p = 250$ km (orbit no. 1 in fig. 22), respectively. Note that this penalty in mission performance is minimal. To obtain a comparable inclination ($i = 75°$) for the 1-Sol orbits, increases of 41.3 percent (orbit no. 8 in fig. 21) and 43.3 percent (orbit no. 7 in fig. 22) in M_i/M_f are required for periapsis altitudes of 500 km and 250 km, respectively.

Therefore, if the arrival characteristics (inclination and eccentricity) of the parking orbit are properly chosen rather than arbitrarily selected, favorable departure conditions (i.e., a tangential periapsis

departure burn) can be obtained that result in lower mass-ratio penalties. Hence, by choosing exact precession orbits, global scientific observations and candidate landing sites can be increased without sacrificing mission performance significantly.

Conclusions

This investigation was initiated to identify trends and aspects of Mars parking orbits for an initial manned mission. This analysis pertained to the following mission profile:

Earth departure	April 4, 2017
Venus swingby	September 9, 2017
Mars arrival	March 23, 2018
Mars departure	May 22, 2018
Earth arrival	November 13, 2018

with Earth departure and arrival velocity increment (ΔV) values of 4.17 km/sec and 1.13 km/sec, respectively, and Mars arrival and departure hyperbolic excess velocity vectors of

Arrival	Departure
$\alpha = 253.99°$	$\alpha = 212.57°$
$\delta = -21.4°$	$\delta = -12.5°$
$V_\infty = 5.441$ km/sec	$V_\infty = 3.873$ km/sec

where α is the angle of right ascension, δ is the angle of declination, and V_∞ is hyperbolic excess velocity. The following conclusions are made:

(1) Precession has a drastic effect on departure ΔV and, hence, on the initial mass in low Earth orbit (LEO). Therefore, a parking orbit cannot be chosen arbitrarily, and a detailed analysis must be performed to obtain an optimum parking orbit.

(2) Both the Mars excursion module (MEM) mass and the overall interplanetary vehicle mass in LEO are insensitive to periapsis altitude of the Mars parking orbit; however, both are sensitive to the inclination and eccentricity of the orbit.

(3) The departure true anomaly must be considered along with inclination and eccentricity of the parking orbit in determining the minimum departure ΔV and, hence, the minimum initial LEO mass.

(4) The choice of parking orbit inclination at Mars should not be limited to direct orbits only. Retrograde orbits can possibly result in lower initial LEO masses, even with the increase in MEM mass associated with their use because of smaller Mars departure ΔV values.

(5) Higher eccentricities (e.g., a 1-Sol orbit) do not necessarily imply minimum initial LEO masses. For some inclinations, a lower eccentricity is favored.

(6) The absolute minimum initial LEO mass was obtained for a highly eccentric parking orbit that did not precess exactly and required a three-dimensional (3-D) departure burn (i.e., a burn with an in-plane and an out-of-plane ΔV component). Therefore, a 3-D departure burn need not imply mission inefficiency.

(7) Minimum initial LEO masses were observed for parking orbits characterized by having near-equatorial inclinations, high eccentricities, and 3-D departure burns. However, because near-equatorial inclination orbits have poor planetary coverage characteristics, they are not desirable from a science viewpoint. Therefore, to enhance the potential for satisfying science requirements, a penalty in mission performance (initial LEO mass) may be imposed. This penalty can be minimized with the use of an exact precession orbit (i.e., an orbit that precesses such that tangential periapsis burns can be performed at both arrival and departure).

(8) The advantage of using an exact precession orbit, in comparison with an orbit that is chosen arbitrarily and requires a 3-D departure burn, is that lower eccentricities and more favorable inclinations (i.e., better scientific requirements) are obtainable without significantly increasing initial LEO mass (i.e., decreasing mission performance). For this mission profile, exact precession orbits were not found to yield the lowest initial LEO mass; however, they may for other manned Mars mission profiles.

In summary, the selection of a final Mars parking orbit, for a particular mission, cannot be based purely on mission performance. A trade-off between the conflicting requirements of mission performance, scientific observations, and landing site accessibility must be made in the selection of an optimum Mars parking orbit.

NASA Langley Research Center
Hampton, VA 23681-0001
October 21, 1992

References

1. Ride, Sally K.: *Leadership and America's Future in Space—A Report to the Administrator.* NASA, Aug. 1987.

2. Braun, Robert D.; Powell, Richard W.; and Hartung, Lin C.: *Effect of Interplanetary Trajectory Options on a Manned Mars Aerobrake Configuration.* NASA TP-3019, 1990.

3. Striepe, Scott A.; Braun, Robert D.; Powell, Richard W.; and Fowler, Wallace T.: Interplanetary Trajectory Optimization of Mars Aerobraking Missions With Constrained Atmospheric Entry Velocities. Paper AAS 91-421, Aug. 1991.

4. Young, Archie C.; Mulqueen, John A.; and Skinner, James E.: *Mars Exploration, Venus Swingby and Conjunction Class Mission Modes, Time Period 2000 to 2045.* NASA TM-86477, 1984.

5. Soldner, John K.: Round-Trip Mars Trajectories. *A Collection of Technical Papers, Part 1—AIAA/AHS Astrodynamics Conference,* Aug. 1990, pp. 497–505. (Available as AIAA-90-2932-CP.)

6. Babb, Gus R.; and Stump, William R.: Mars Orbit Selection. *Manned Mars Missions,* NASA TM-89320, 1986, pp. 78–86.

7. Stump, William R.; Babb, Gus R.; and Davis, Hubert P.: Mars Lander Survey. *Manned Mars Missions,* NASA TM-89320, 1986, pp. 239–251.

8. Tucker, Michael; Meredith, Oliver; and Brothers, Bobby: Space Vehicle Concepts. *Manned Mars Missions,* NASA TM-89320, 1986, pp. 316–341.

9. Walberg, Gerald D.: A Review of Aerobraking for Mars Missions. Paper No. IAF 88-196, Oct. 1988.

10. Mead, Charles W.; and Jones, Max F.: *Optimization of "Ephemeridal" Parameters for Minimum Propellant Requirements on Multiplanet Roundtrip Swingby-Stopover Missions.* TM 54/30-189 (Contract NAS8-20082), Lockheed Missiles & Space Co., May 1968.

11. Tolson, Robert H.: *Geometrical Characteristics of Lunar Orbits Established From Earth-Moon Trajectories.* NASA TN D-1780, 1963.

12. Canetti, G. S.: *Final Report—Definition of Experimental Tests for a Manned Mars Excursion Module. Volume II—Design.* SD 67-755-2 (Contract NAS9-6464), Space Div., North American Rockwell Corp., Jan. 12, 1968. (Available as NASA CR-65912.)

13. Bate, Roger R.; Mueller, Donald D.; and White, Jerry E.: *Fundamentals of Astrodynamics.* Dover Publ., Inc., 1971.

14. Christensen, Edward J.; and Balmino, Georges: Development and Analysis of a Twelfth Degree and Order Gravity Model for Mars. *J. Geophys. Res.,* vol. 84, no. B14, Dec. 30, 1979, pp. 7943–7953.

15. Gapcynski, J. P.; Tolson, R. H.; and Michael, W. H., Jr.: Mars Gravity Field: Combined Viking and Mariner 9 Results. *J. Geophys. Res.,* vol. 82, no. 28, Sept. 30, 1977, pp. 4325–4327.

16. Daniels, Edward F.; Tolson, Robert H.; and Gapcynski, John P.: Spherical Harmonic Representation of the Martian Gravity Using a Short-Arc Technique. *J. Spacecr. & Rockets,* vol. 14, no. 6, June 1977, pp. 323–327.

17. Kaula, William M.: *Theory of Satellite Geodesy—Applications of Satellites to Geodesy.* Blaisdell Publ. Co., c.1966.

18. Brauer, G. L.; Cornick, D. E.; and Stevenson, R.: *Capabilities and Applications of the Program To Optimize Simulated Trajectories* (POST)*—Program Summary Document.* NASA CR-2770, 1977.

19. Desai, Prasun N.; and Buglia, James J.: Determination of Precessing Mars Parking Orbits Which Insure In-Plane Arrival and Departure Burns. Paper AAS 91-117, Feb. 1991.

20. Desai, Prasun N.; and Buglia, James J.: Arrival and Departure Impulsive ΔV Determination for Precessing Mars Parking Orbits. Paper AAS 92-102, Feb. 1992.

21. Desai, Prasun N.; and Buglia, James J.: Determining Mars Parking Orbits Which Ensure Tangential Periapsis Burns at Arrival and Departure. AIAA-92-4582, Aug. 1992.

22. Young, Archie C.: Mission and Vehicle Sizing Sensitivities. *Manned Mars Missions,* NASA TM-89320, 1986, pp. 87–102.

Table 1. Estimate of Vehicle Dry Mass

Vehicle component	Mass, kg
Two habitation modules (ref. 8)	43 200
Truss structure and support equipment (ref. 2)	11 000
Earth return capsule (ref. 9)	6 800
MEM	34 000–82 400
Total mass at Mars arrival	95 000–143 400
Total mass at Mars departure	61 000
Total mass at Earth arrival	6 800

Table 2. MEM Characteristics

Initial dry mass before deorbiting (ref. 7), kg	21 400
Final dry mass after rendezvous (ref. 7), kg	2420
Liftoff T/W (on Mars)	1.3
Reference diameter (ref. 7), m	9.754
Length of stay time, days	60
Crew (ref. 7)	4
I_{sp} (ref. 7), sec	360.5

Table 3. Effect of Oblateness Upon Mission Performance

Parking orbit analysis conditions	Parking orbit characteristics	ΔV_{ins}, km/sec	ΔV_{dep}, km/sec	Departure burn direction	Initial LEO mass, kg $\times 10^6$
Neglecting precession	$i = 90°$ $e = 0.809$ $h_p = 500$ km	2.72	1.62	Assumed tangential $\theta = 0°$	0.921
Including precession	$i = 90°$ $e = 0.809$ $h_p = 500$ km	2.72	4.27	$\gamma = 30°$ $\beta = 90°$ $\theta = 0°$	1.42

Table 4. Potential Parking Orbits for a Periapsis Altitude of 500 km

	Parking orbit number	Parking orbit characteristics	ΔV_{ins}, km/sec	ΔV_{dep}, km/sec	Departure burn direction	Mass ratio in LEO, M_i/M_f	Mass in LEO, kg
Exact precession results	1	$i = 70.7°$ $e = 0.381$	3.28	2.18	Tangential $\theta = 0°$	145.3	0.9880×10^6
	2	$i = 135.7°$ $e = 0.225$	3.51	2.43	Tangential $\theta = 0°$	155.9	1.060
	3	$i = 51.5°$ $e = 0.0992$	3.71	2.63	Tangential $\theta = 0°$	162.9	1.108
	4	$i = 133.7°$ $e = 0.0358$	3.81	2.71	Tangential $\theta = 0°$	170.1	1.157
	5	$i = 129.2°$ $e = 0.0125$	3.85	2.76	Tangential $\theta = 0°$	172.1	1.170
Other results of interest	6	$i = 158.5°$ $e = 0.809$	2.72	1.66	$\gamma = 6.3°$ $\beta = 6.4°$ $\theta = 336°$	141.5	0.9622
	7	$i = 21.5°$ $e = 0.809$	2.72	2.69	$\gamma = 29.4°$ $\beta = 21.2°$ $\theta = 240°$	152.9	1.040
	8	$i = 75°$ $e = 0.809$	2.72	4.10	$\gamma = 21.3°$ $\beta = 89.5°$ $\theta = 311°$	199.5	1.360
	9	$i = 90°$ $e = 0.809$	2.72	4.25	$\gamma = 26.5°$ $\beta = 91.8°$ $\theta = 350°$	206.7	1.406

Table 5. Potential Parking Orbits for a Periapsis Altitude of 250 km

	Parking orbit number	Parking orbit characteristics	ΔV_{ins}, km/sec	ΔV_{dep}, km/sec	Departure burn direction	Mass ratio in LEO, M_i/M_f	Mass in LEO, kg
Exact precession results	1	$i = 71.1°$ $e = 0.436$	3.18	2.10	Tangential $\theta = 0°$	138.9	0.9445×10^6
	2	$i = 21.6°$ $e = 0.1684$	3.58	2.50	Tangential $\theta = 0°$	155.1	1.055
	3	$i = 105.3°$ $e = 0.053$	3.77	2.71	Tangential $\theta = 0°$	166.2	1.130
	4	$i = 119°$ $e = 0.005$	3.85	2.75	Tangential $\theta = 0°$	168.3	1.144
Other results of interest	5	$i = 158.5°$ $e = 0.821$	2.66	1.65	$\gamma = 8.5°$ $\beta = 9.6°$ $\theta = 330°$	138.8	0.9438
	6	$i = 21.5°$ $e = 0.821$	2.66	2.71	$\gamma = 30.2°$ $\beta = 21.9°$ $\theta = 236.9°$	150.7	1.025
	7	$i = 75°$ $e = 0.821$	2.66	4.18	$\gamma = 21.9°$ $\beta = 90.7°$ $\theta = 310°$	199.0	1.353
	8	$i = 90°$ $e = 0.821$	2.66	4.36	$\gamma = 27.6°$ $\beta = 93.2°$ $\theta = 351°$	207.6	1.412

Figure 1. Baseline configuration of interplanetary transfer vehicle (ref. 2).

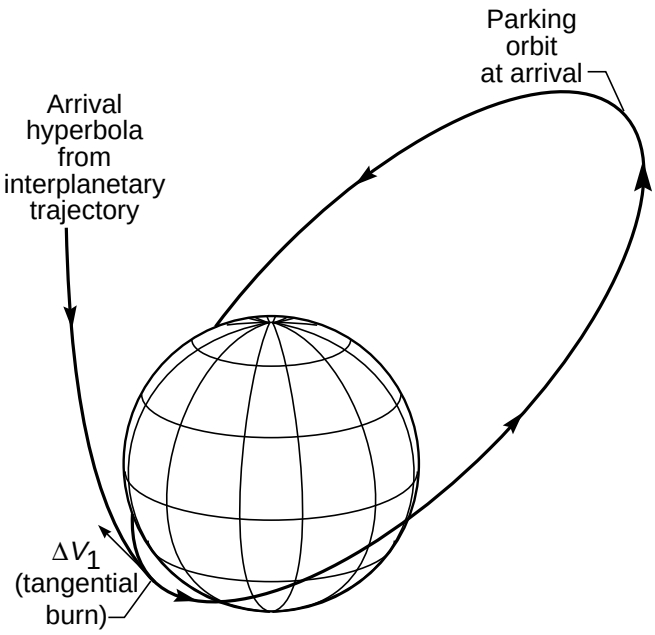

(a) Upon Mars arrival.

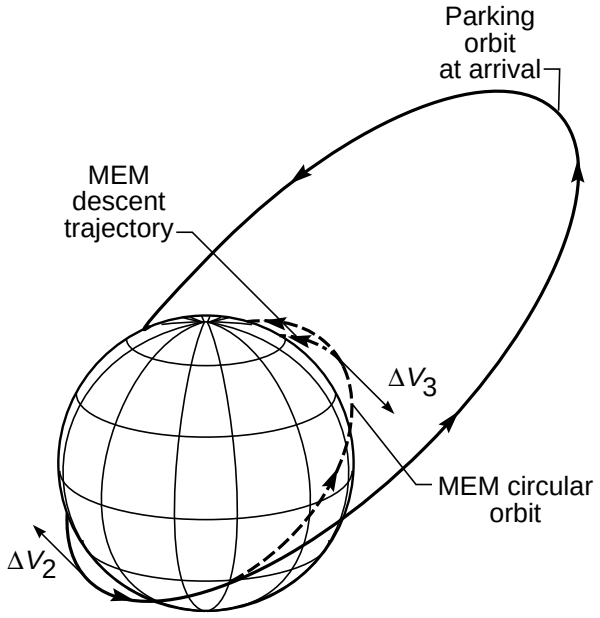

(b) Upon Mars descent.

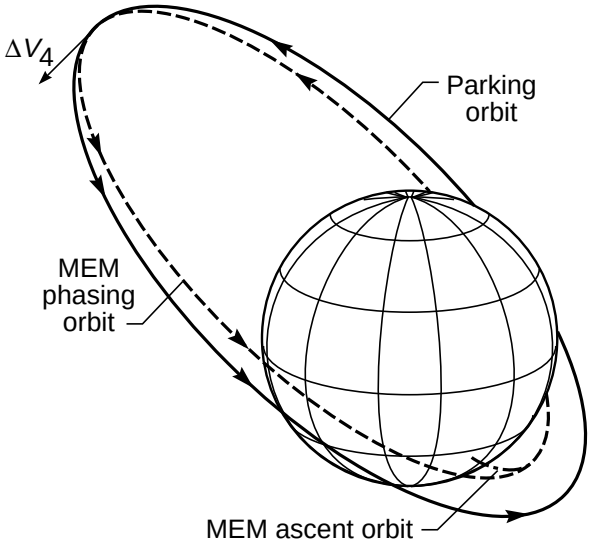

(c) Upon Mars ascent.

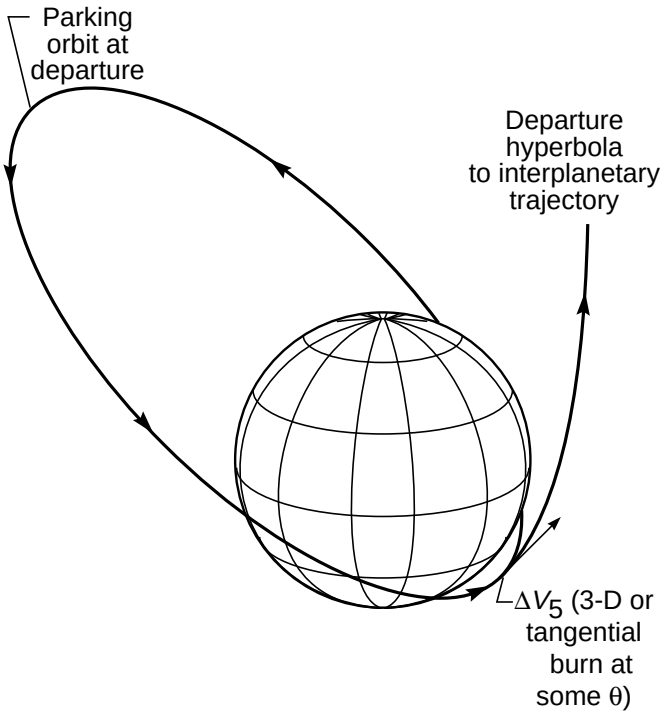

(d) Upon Mars departure.

Figure 2. Mission geometries.

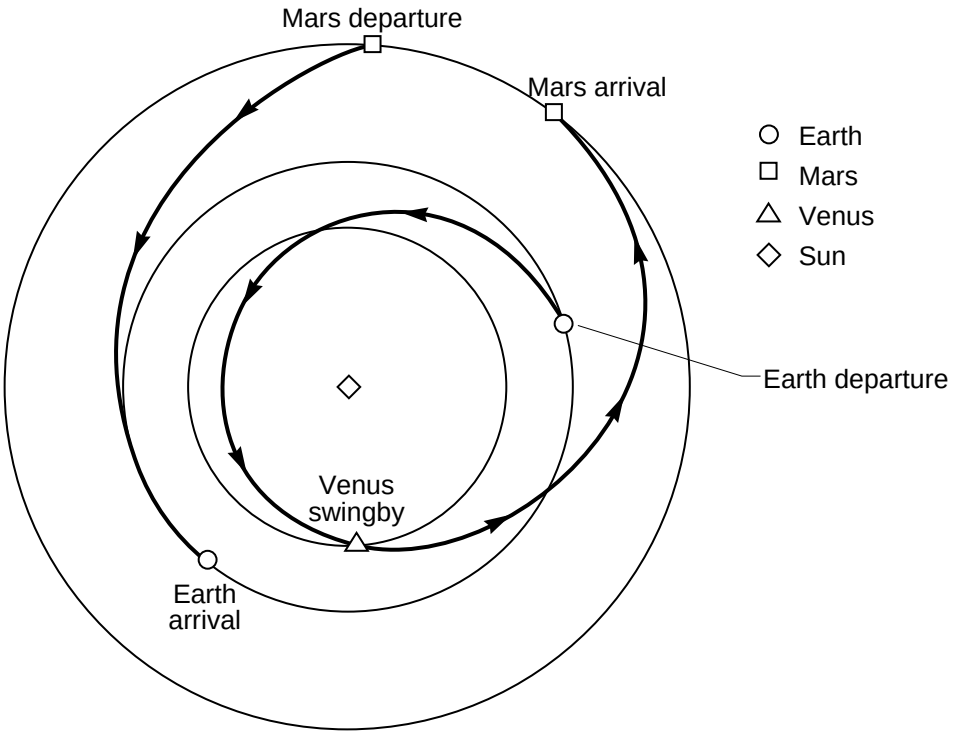

Figure 3. Heliocentric trajectory of baseline mission.

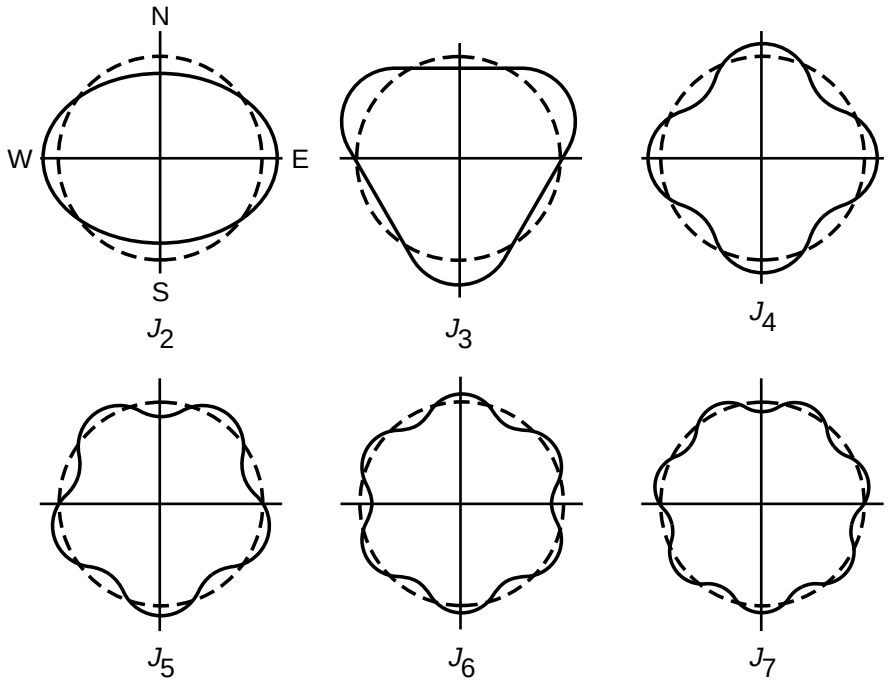

Figure 4. Geometrical shape of the Legendre polynomials corresponding to the zonal coefficients.

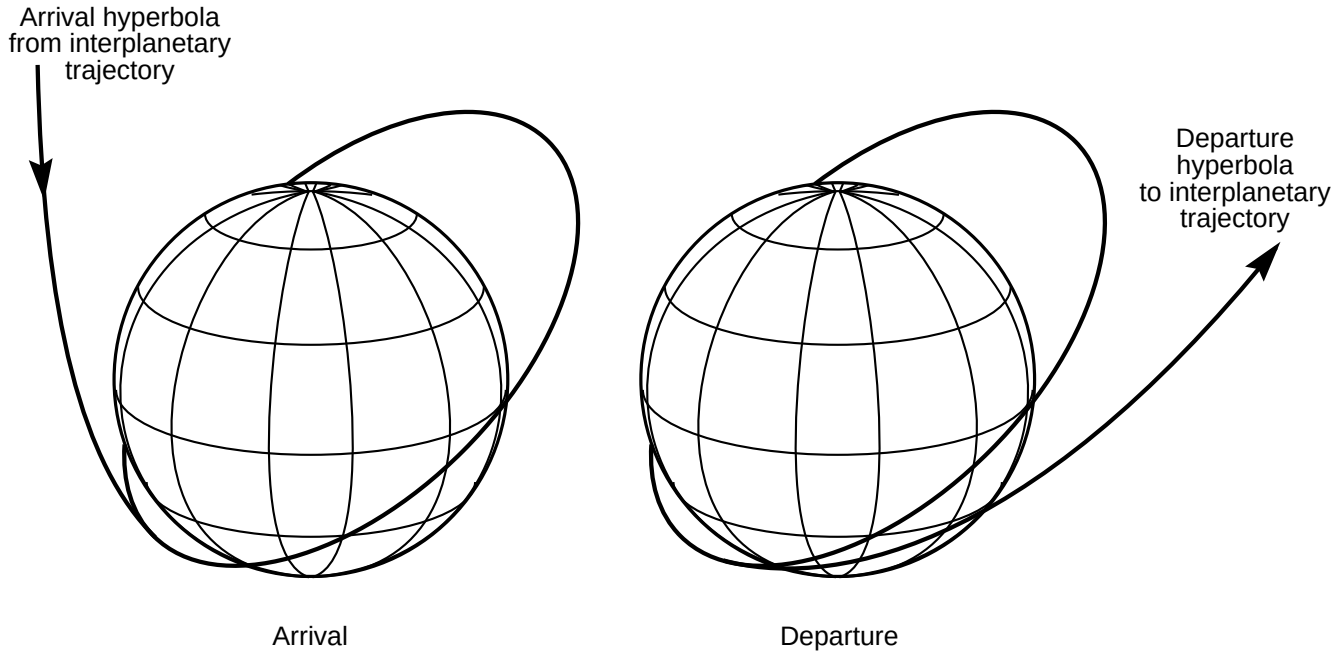

Figure 5. Geometry between the parking orbit and the interplanetary trajectory for a spherical Mars.

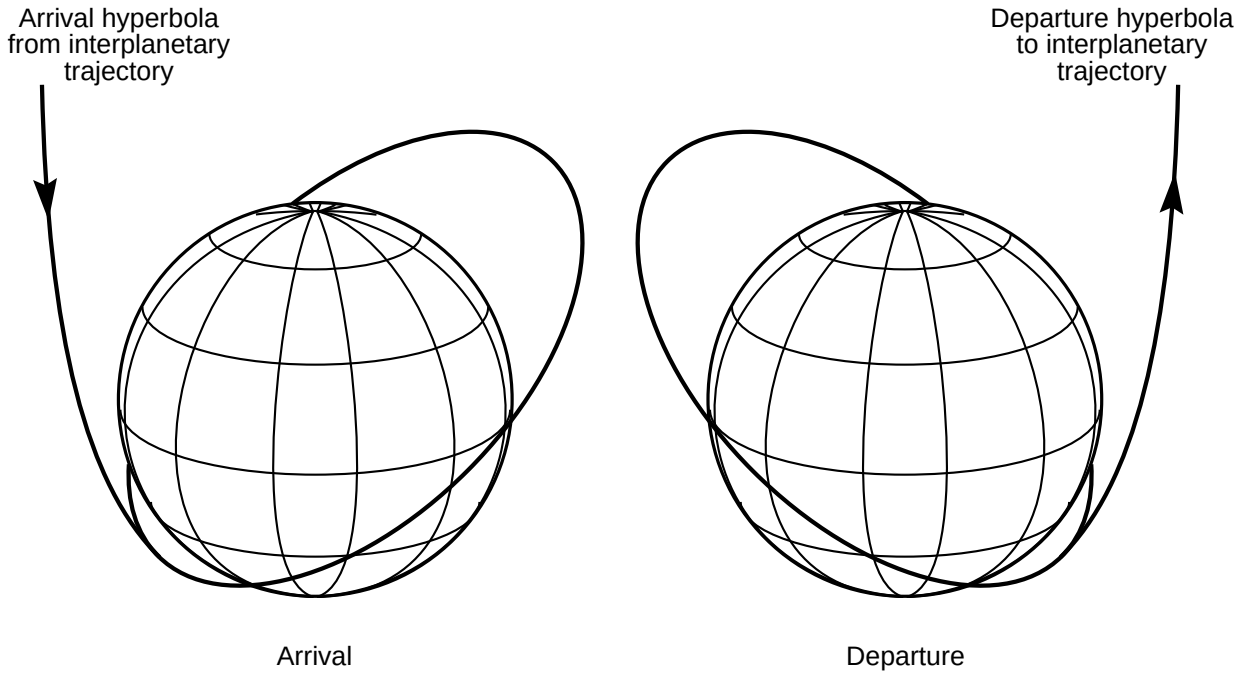

Figure 6. Geometry between the parking orbit and the interplanetary trajectory for an oblate Mars.

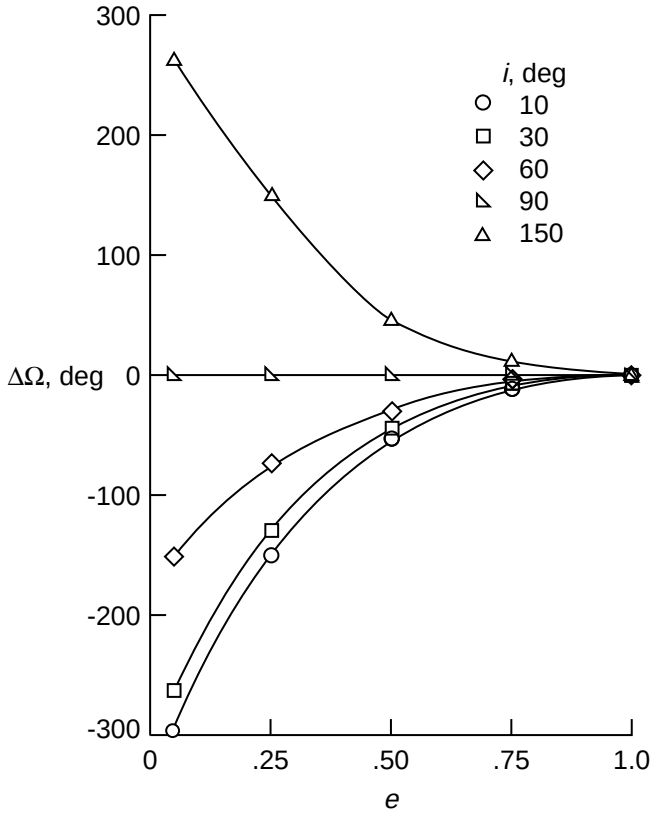

Figure 7. Change in Ω for a 30-day Mars stay time ($h_p = 250$ km).

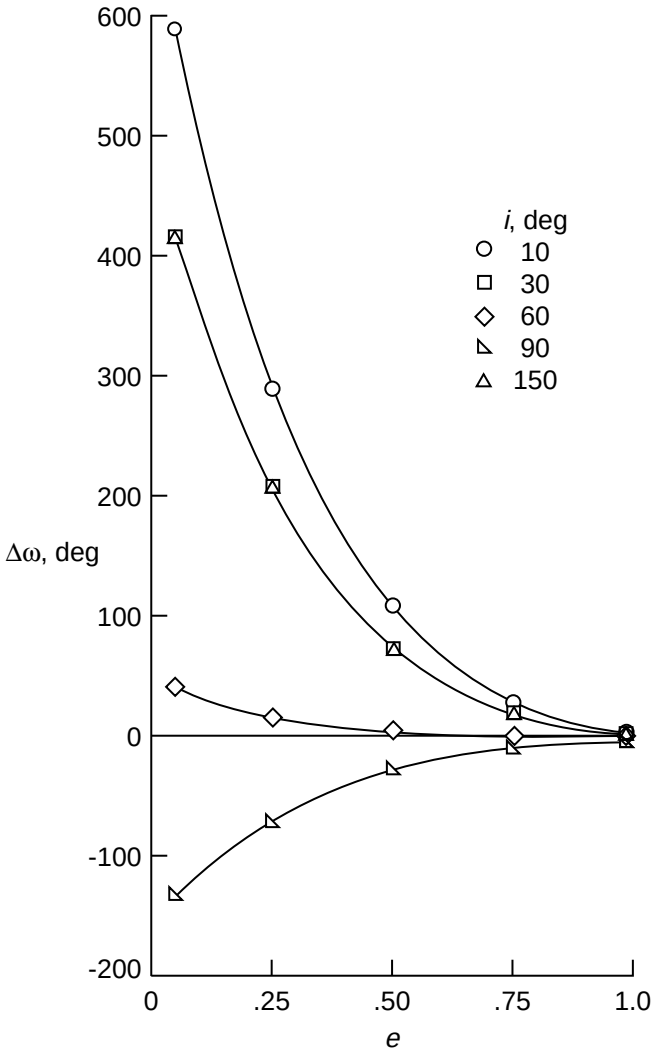

Figure 8. Change in ω for a 30-day Mars stay time ($h_p = 250$ km).

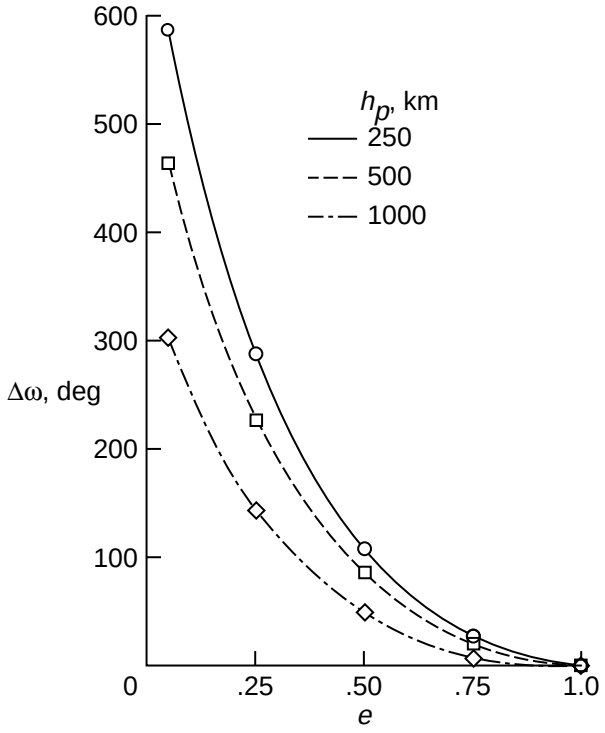

Figure 9. Change in ω for a 30-day Mars stay time ($i = 10°$).

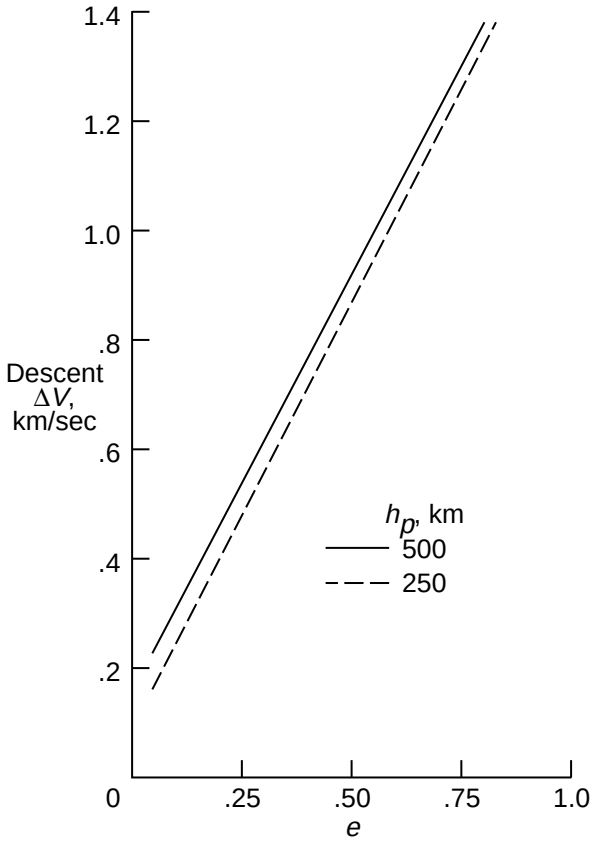

Figure 10. MEM descent ΔV.

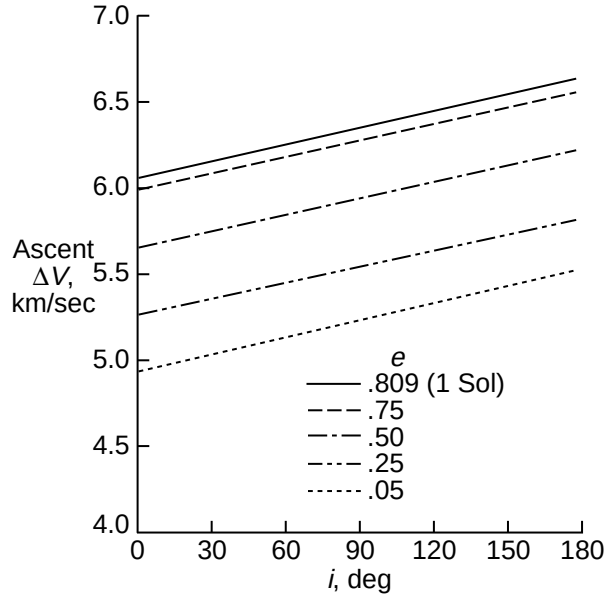

Figure 11. MEM ascent ΔV for $h_p = 500$ km.

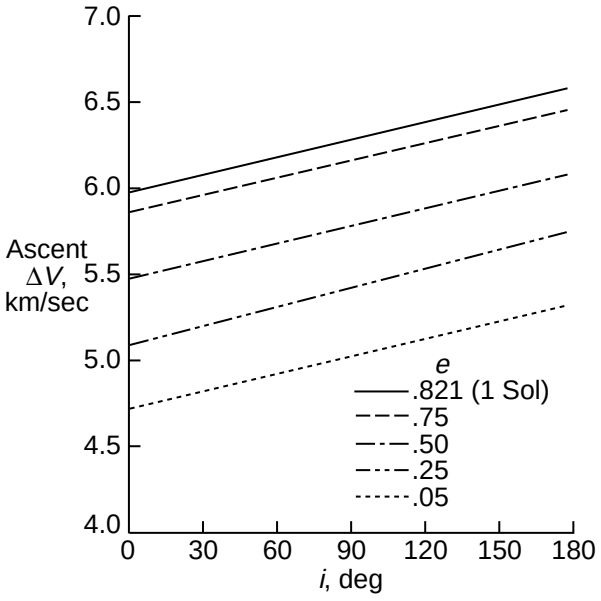

Figure 12. MEM ascent ΔV for $h_p = 250$ km.

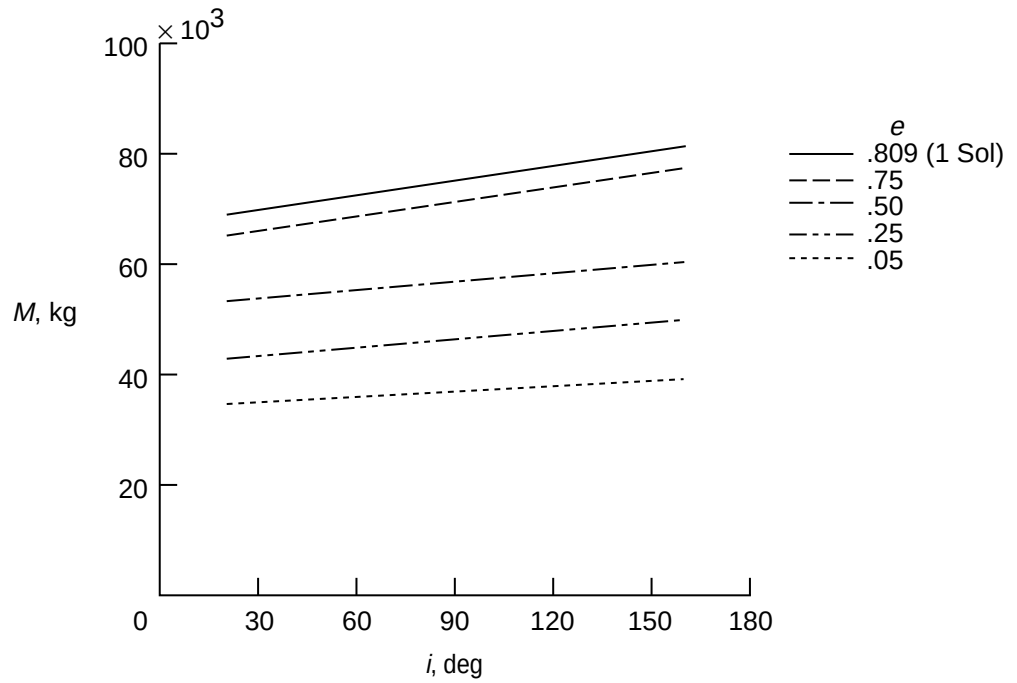

Figure 13. MEM mass for $h_p = 500$ km.

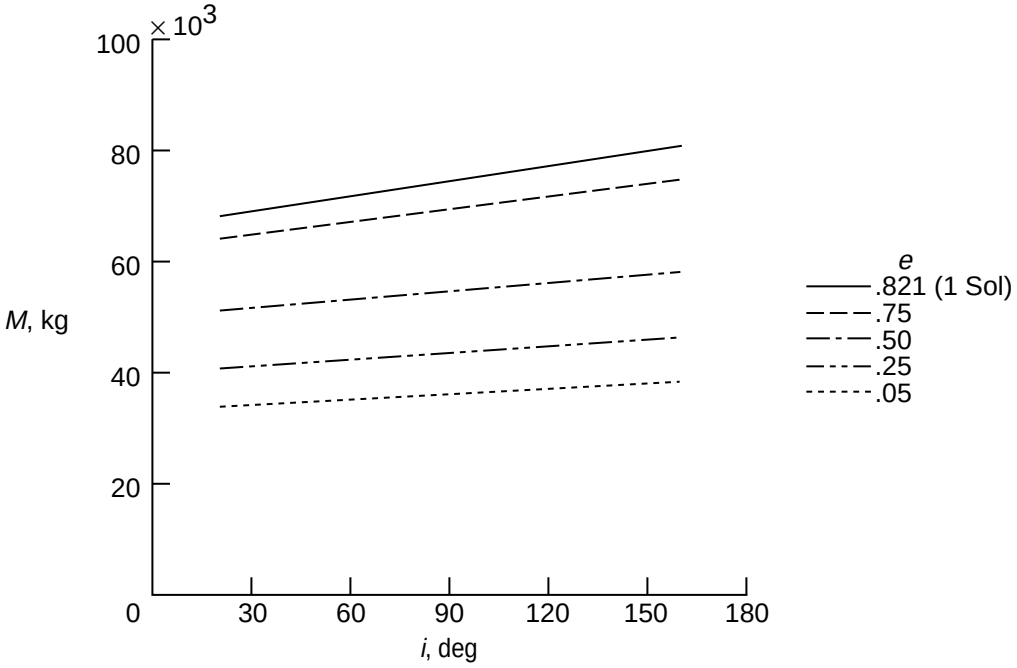

Figure 14. MEM mass for $h_p = 250$ km.

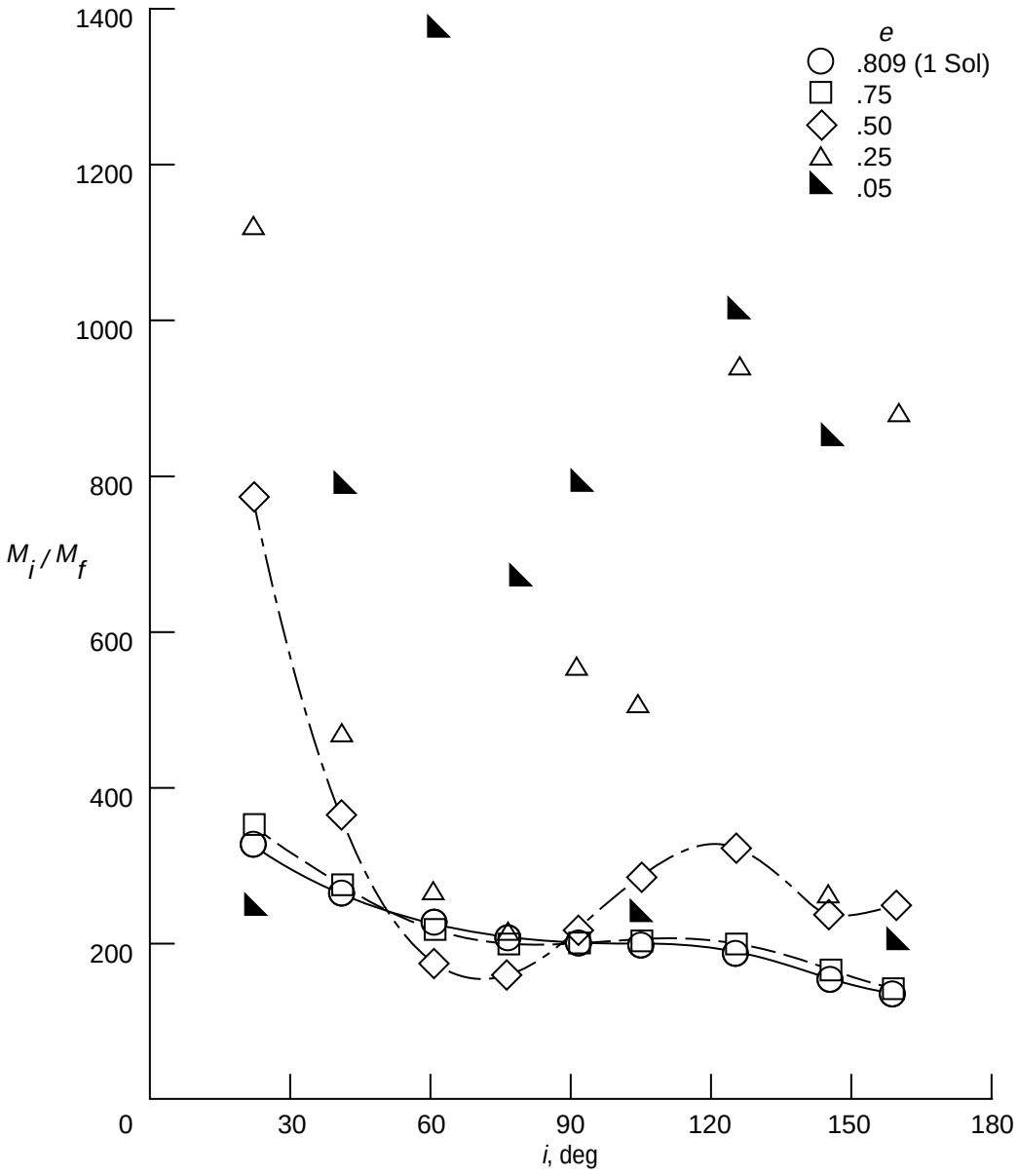

Figure 15. Mass ratio in LEO with a periapsis departure ($h_p = 500$ km).

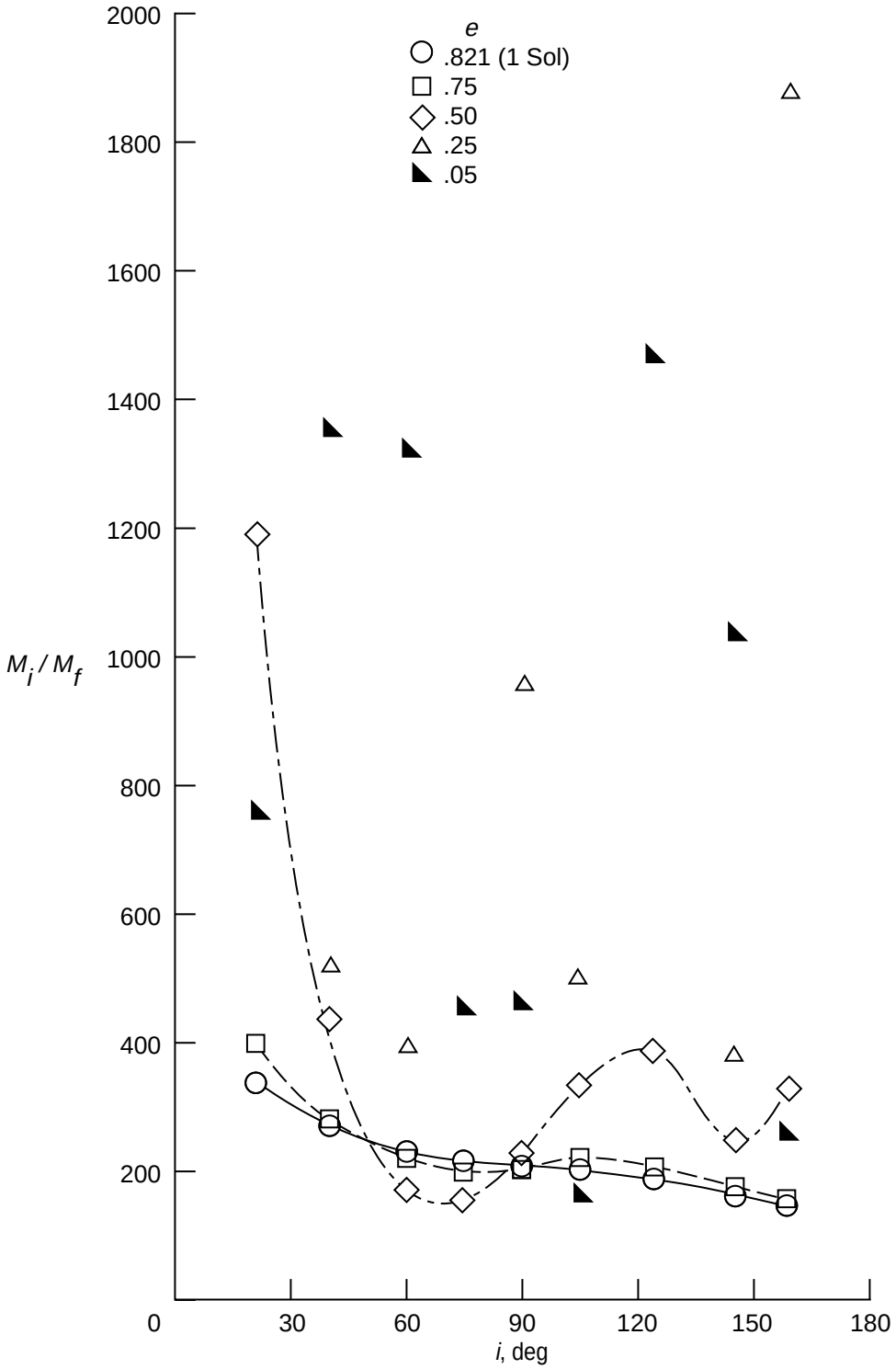

Figure 16. Mass ratio in LEO with a periapsis departure ($h_p = 250$ km).

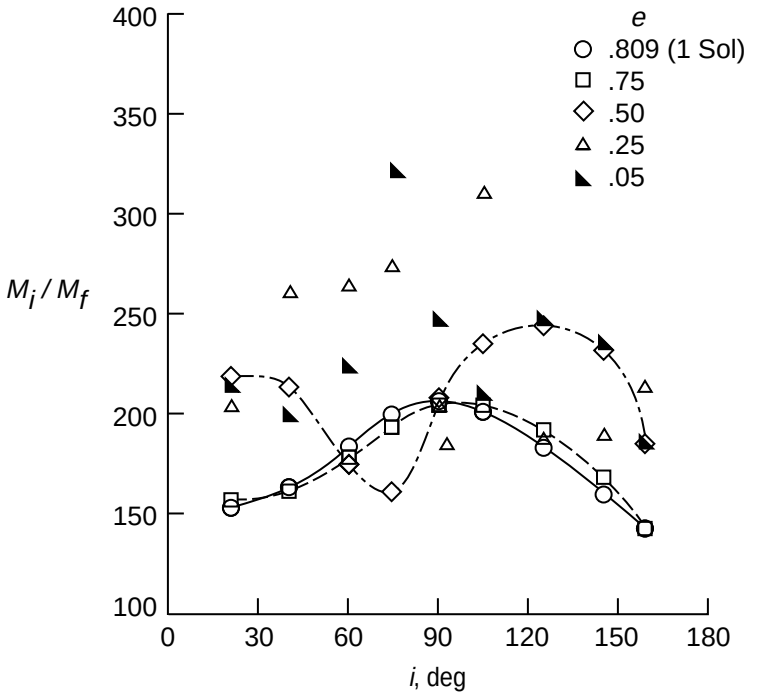

Figure 17. Mass ratio in LEO with an optimized departure ($h_p = 500$ km).

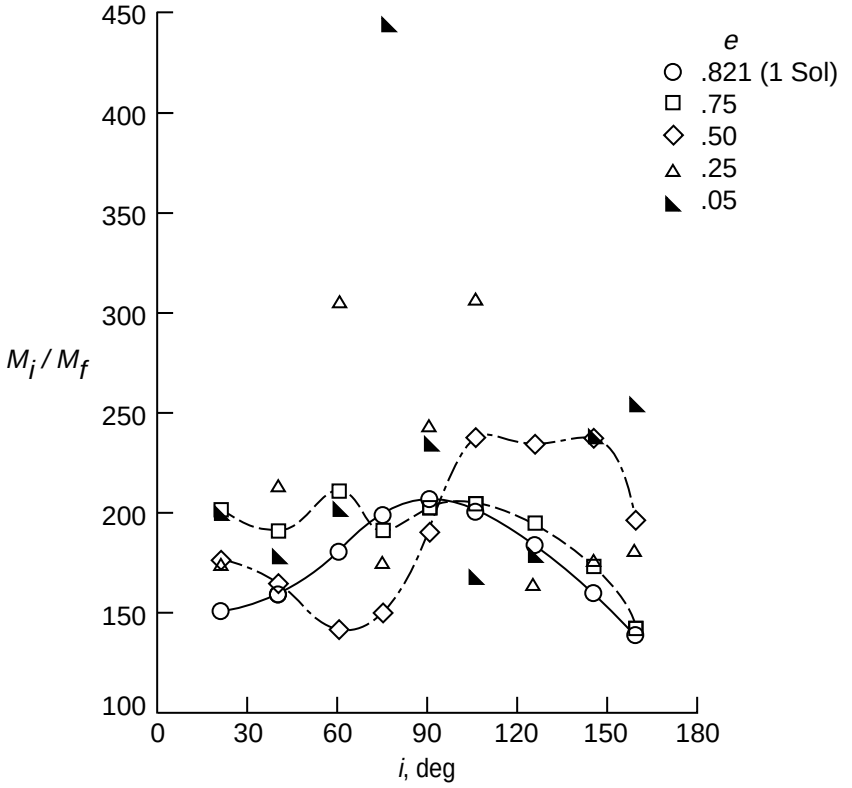

Figure 18. Mass ratio in LEO with an optimized departure ($h_p = 250$ km).

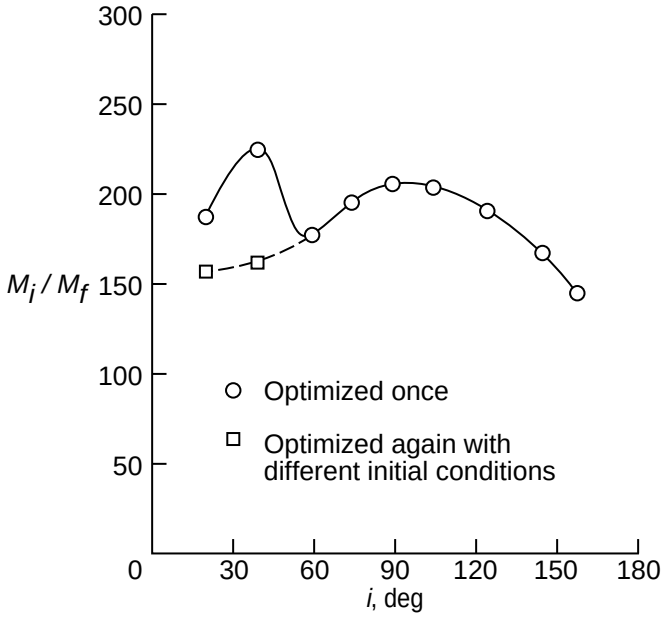

Figure 19. Change in mass ratio in LEO caused by local optimums ($h_p = 500$ km, $e = 0.75$).

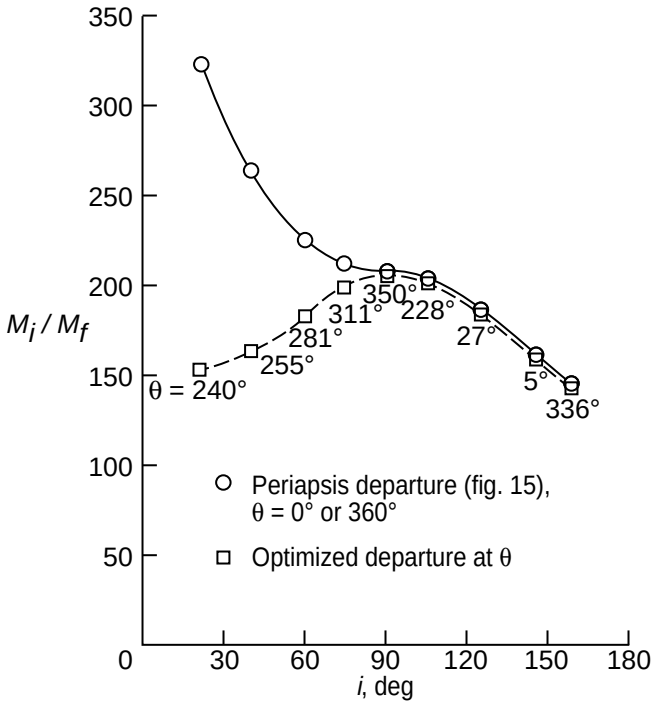

Figure 20. Comparison of mass ratio in LEO between a periapsis departure and an optimized departure location ($h_p = 500$ km, $e = 0.809$).

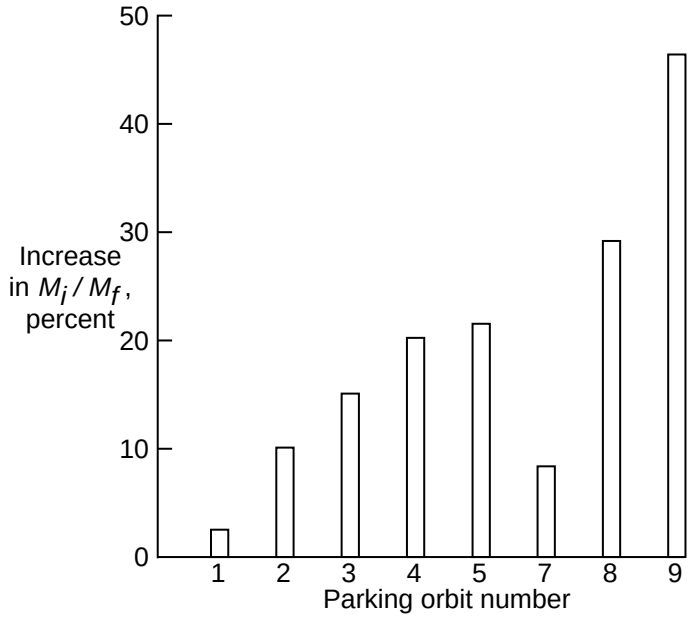

Figure 21. Percent increase in LEO mass ratio for various parking orbits ($h_p = 500$ km).

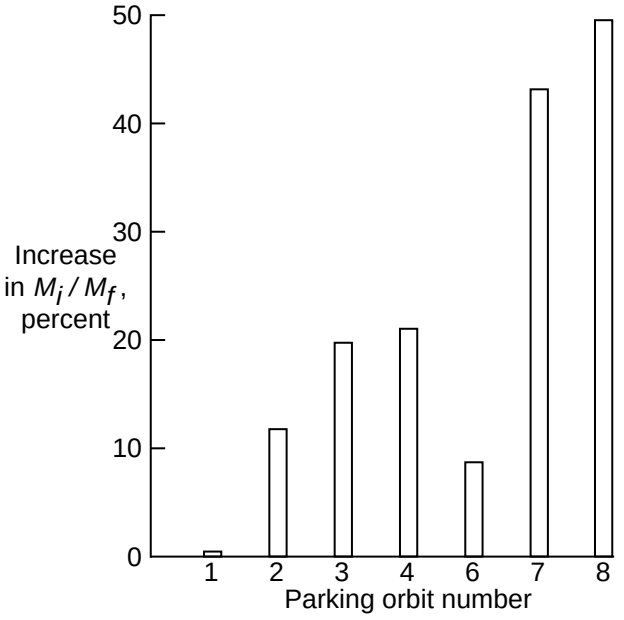

Figure 22. Percent increase in LEO mass ratio for various parking orbits ($h_p = 250$ km).

Figure 1. Baseline configuration of interplanetary transfer vehicle (ref. 2).